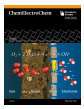

# Experimental and Model-Based Analysis of Electrolyte Intrusion Depth in Silver-Based Gas Diffusion Electrodes

David Franzen,* Christian Krause, and Thomas Turek*[a]

The electrolyte distribution is a central point of discussion for understanding the processes inside gas-diffusion electrodes (GDE) for the oxygen reduction reaction in highly alkaline media. During first radiographic operando synchrotron experiments, the liquid electrolyte was located, however, the through-plane distribution remains unclear. Therefore, model electrodes consisting of nickel and silver layers are developed to determine the electrolyte intrusion depth. Nickel-based GDEs are modified to achieve a pore system morphology suitable for the oxygen reduction reaction and subsequently coated with silver-PTFE catalyst layers. These graded electrodes form gas-diffusion (nickel) and reaction (silver) layers. The electrodes performance is determined under industrial conditions (80 °C, 30 wt% NaOH electrolyte) as a function of the silver layer thickness and thus of the effective intrusion depth of the electrolyte. The model-based analysis confirms the experimental determined intrusion depths. Nevertheless, additional operando tomography measurements would help to further improve the understanding of the processes inside GDE.

## 1. Introduction

Chlorine is one of the most important basic materials for the chemical industry, which is mainly produced by the very energy intensive chlor-alkali electrolysis.[1] By introducing the so-called oxygen depolarized cathode (ODC) to the state-of-the art membrane process, electrical energy savings of up to 25% are obtained.[2] The ODC consumes oxygen and suppresses the hydrogen evolution reaction, which results in a reduction of the required cell voltage of up to 1 V. Due to the low solubility of oxygen at operation conditions (80 °C, 30–32 wt% NaOH),[3] the ODC is designed as a gas-diffusion electrode (GDE). The GDE consist of an electrocatalyst and a hydrophobic binder, allowing the electrolyte to intrude the electrode, but provide enough hydrophobicity to prevent a complete flooding of the electrode. In this way, a complex electrolyte distribution inside the GDE is formed, determining the three-phase boundary and thus the available surface area for the electrochemical reaction. Therefore, precise knowledge of the electrolyte distribution within GDE is fundamental. In industrial ODCs, silver is utilized as the electrocatalyst, as the oxygen reduction reaction (ORR) activity on silver is comparable to platinum at the given process conditions.[4] Operando experiments are extremely challenging, as the high silver content leads to a high absorption of X-ray or synchrotron radiation. Until now only radiographic images of the electrolyte distribution inside an ODC during operation are available.[5–7] Unfortunately, these measurements do not provide sufficient information about the penetration depth of the electrolyte.

To further improve the understanding of processes inside GDE, we developed a so-called thin-film flooded agglomerates (TFFA) model, described in detail in our previous publication.[7] This model, developed on the basis of the work of Cutlip,[8] Wang and Koda[9,10] and Pinnow et al.,[11] describes the ORR in a porous silver-based GDE for the first time with a realistic electrolyte distribution based on operando experiments. However, the penetration depth of the electrolyte remains unknown. In experimental studies, a droplet formation on the gas side of the electrode is observed,[5,6,12] and identified to contain electrolyte[13] and not only condensed water vapor. These findings indicate that the electrolyte intrudes over the full thickness of the electrode. Furthermore, Frania[14] showed with his model electrodes, consisting of silver dendrites in polytetrafluoroethylene (PTFE) membranes, that the silver catalyst is utilized within the entire electrode. However, these membrane-supported electrodes have a completely different structure than conventional GDE made from silver and PTFE particles. While Kunz et al.[15] hardly found any electrolyte imbibition in a silver-based pore system without application of a large differential pressure in their simulations, Röhe et al.[16,17] determined small intrusion depths of the electrolyte based on their dynamic model approach. In summary, quite contradictory information can be found in the literature, although the electrolyte distribution and the penetration depth is of fundamental importance for understanding the processes in GDE with liquid electrolyte. As long as no reliable operando tomography data is available, other indirect methods must be employed.

In a recent study Gebhard et al.[18] tried to prevent a too deep electrolyte intrusion by barrier layers inside the GDE. However, the reported performance boost contradicts our model-based analysis, according to which a larger penetration

[a] D. Franzen, C. Krause, Prof. Dr. T. Turek
Institute of Chemical and Electrochemical Process Engineering
Clausthal University of Technology
Leibnizstraße 17, 38678 Clausthal-Zellerfeld, Germany
E-mail: franzen@icvt.tu-clausthal.de
turek@icvt.tu-clausthal.de

Supporting information for this article is available on the WWW under https://doi.org/10.1002/celc.202100278

depth should enhance the electrode performance, and is presumably due to percolation processes inside the special electrode with barrier layer. In a new approach, we therefore manufactured graded electrodes consisting of two layers made of different materials. Nickel-PTFE, which is catalytically almost inactive towards the ORR,[19] is used as additional diffusion layer, which is coated with a standard silver-PTFE layer. During operation, the electrolyte will likely spread through the graded electrodes with a distribution similar to a standard full silver-PTFE GDE. However, the electrochemical reaction will only take place at the catalytically active silver part. In this way we are able to investigate the effect of the catalyst layer thickness, and thus the effective intrusion depth of the electrolyte, experimentally and can compare the results with our TFFA-model approach.

## 2. Results and Discussion

### 2.1. Analysis of the Pore System

In a previous publication, we already presented the importance of an appropriate pore system for the performance of GDEs.[20] Therefore, we tried to prepare nickel and silver layers with comparable pore systems. Koj et al.[21] reported mean pore diameters of approximately 2 µm and a wide distribution of up to 10 µm for pure nickel GDEs. For the oxygen reduction reaction (ORR) in silver-based electrodes, pore diameters of 0.7 µm are best suited. In order to obtain similar pore networks for the nickel and silver layers, the recipe for the nickel suspension is modified as described in the experimental section. Additionally, an intermediate pressing step decreases the pore size of the pure nickel electrodes to a mean value of 1 µm with largest pores having sizes smaller than 2 µm, a reduction of roughly 8 µm. In this way, nickel layers, close to the properties of the silver layer can be produced. The pore size distributions for all electrodes obtained by capillary-flow porometry are shown in Figure 1. With loadings above 30 $mg_{Ag}\,cm^{-2}$ the pore system is primarily defined by the silver layer. Mean pore sizes are similar to the pure silver GDE (136 $mg_{Ag}\,cm^{-2}$), only the shape of the distribution is slightly influenced by the nickel layer (see results for the pure nickel GDE). The distribution of the pure nickel electrode and the electrode with a loading of 15 $mg_{Ag}\,cm^{-2}$ is almost identical. We assume that the silver layer is not completely dense, leading to preferred pathways and channeling effects through the catalyst layer. Thus the pore size distribution is primarily defined by the nickel layer. However, for the electrochemical characterization these channeling effects are secondary, as there is no differential pressure between electrolyte and gas compartment during the experiments. Overall, we assume that the electrolyte distribution in the individual electrode areas, nickel and silver layers, does not deviate significantly from each other. Thus, the thickness of the silver layer should define the catalytically active area for the ORR. This allows us to drawn direct conclusions about the effective penetration depth of silver electrodes.

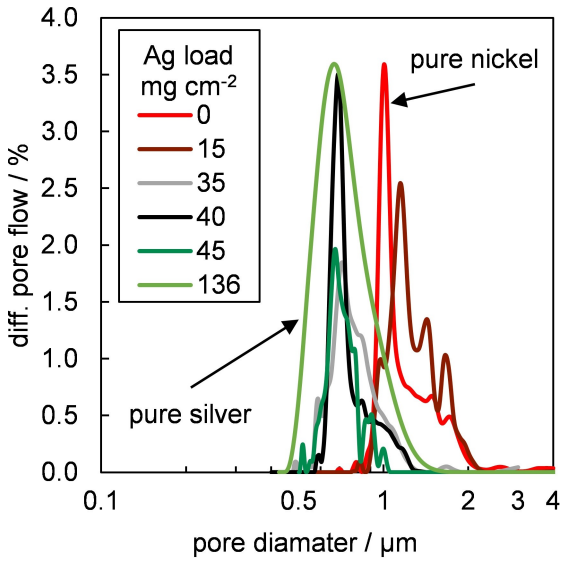


**Figure 1.** Pore size distribution for GDE with different silver loadings.

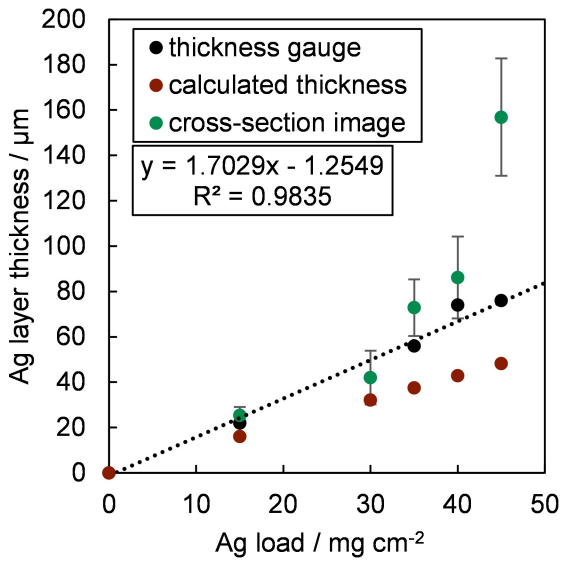


**Figure 2.** Silver layer thickness as a function of the silver loading determined by different evaluation methods.

### 2.2. Layer Thickness Analysis

The thickness of the silver layer is determined by a nine-point measurement with a thickness gauge after the intermediate pressing step and final sintering of the electrode. This should yield reliable results since the sintering process hardly influences the total thickness of the electrode. In a second approach, thicknesses of the silver layer are calculated with the applied silver loading and the experimentally determined true density of pure silver GDE,[20] assuming a linear correlation between silver loading and layer thickness. The values calculated in this way are lower than those measured with the thickness gauge (Figure 2). However, the determination of the silver loading is influenced by the average mass loss of the GDE during the

sintering process, as the silver layers are applied on wet nickel electrodes. An exact determination of the dry silver load by weighing is therefore not possible due to the production procedure. Furthermore, the influence of the contact line between nickel and silver layers on the true density of the silver layer is unknown. Such effects cannot be ruled out, as deviations between expected and true density were already observed in our previous studies.[20] In a third approach, the layer thicknesses are determined by cross-sectional images at different positions of the electrode (see Figure 2 and also Figure 6 in the experimental section). Except for the highest silver loading of 45 mg cm$^{-2}$, the values from thickness gauge and cross-section images are in quite good agreement. However, the error bars for the imaging method indicate the relatively large uncertainties of this method. Moreover, especially at higher loadings, a deformation of the silver layer during the cutting process might take place. Taking all factors into account, the measurements with the thickness gauge should be the most precise. Overall, the goal to prepare silver layers with different thickness on top of a nickel layer with comparable pore structure could be successfully reached.

### 2.3. ORR Activity of Graded Electrodes

The *iR*-compensated polarization curves for all investigated electrodes are shown in Figure 3. As expected, a pure nickel electrode shows a very poor performance towards the ORR in both, the linear and the kinetic region. The limiting current density is only 0.5 kA m$^{-2}$ and in the kinetic region, the overpotential is approximately 200 mV higher than for all silver-containing electrodes. Already the lowest silver loading of 15 $mg_{Ag}$ cm$^{-2}$ shifts the overpotential in the kinetic region down to 100 mV, showing the improved catalytic activity of the electrode. However, the performance is still limited by the available three-phase boundary as the limiting current density rises to only 1.2 kA m$^{-2}$. Doubling the loading to 30 $mg_{Ag}$ cm$^{-2}$ increases the current density further to 2.7 kA m$^{-2}$. Even higher loadings lead to a strong reduction of the overpotentials and to much higher limiting current densities. All electrodes with loadings above 35 $mg_{Ag}$ cm$^{-2}$ are capable to provide an industrially relevant current density of 4 kA m$^{-2}$. The electrode with a loading of 45 $mg_{Ag}$ cm$^{-2}$ exhibits overpotentials very similar to the pure silver electrode. The only difference is the limiting current density, which is reached at 7.9 kA m$^{-2}$, while the pure silver electrode does not show any limitations within the investigated range of up to 10 kA m$^{-2}$. In the kinetic region, a similar effect is observed. For the GDEs with a loading of 15, 30 and 45 $mg_{Ag}$ cm$^{-2}$, a gradual decrease of the overvoltage by approximately 25 mV is observed. The GDEs with loadings of 35 and 40 $mg_{Ag}$ cm$^{-2}$, as well as the pure silver electrode, show slightly higher overvoltages. Overall, the trend here seems to be similar to that in the linear region, higher catalyst loadings will lead to lower overpotentials. The inconsistency here is likely to be explained by the hand spraying process. The reproducibility of the electrodes properties is very high, but not perfect. However, this affects the kinetic region more than the linear range and limiting current densities. Further, smaller deviations between the curves of the pure silver and the graded electrodes may occur, as the pore system of the nickel layer is comparable to, but not identical with that of the silver layers. Therefore, there may be slight differences in the electrolyte distribution, which will be neglected in the model-based analysis.

### 2.4. Model-Based Analysis

In a first attempt, the silver layer thicknesses determined by the gauge are implemented in the model as the length of the reaction zone, which is intruded by the electrolyte. In reality, as mentioned above, the electrolyte will intrude the nickel layer as well. However, the nickel surface does not contribute to the

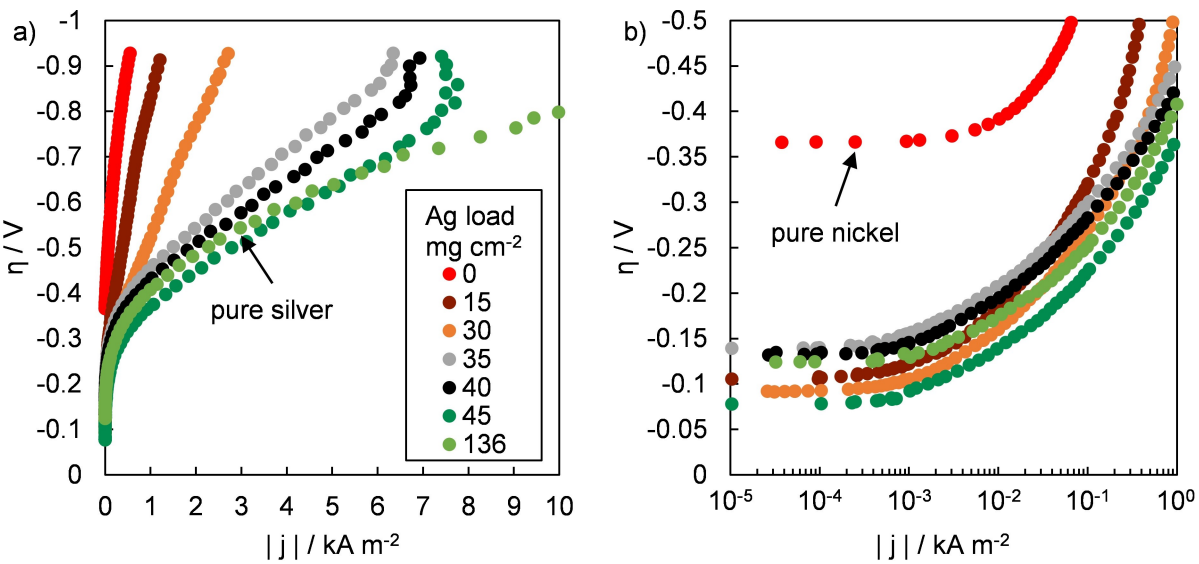


**Figure 3.** Polarization curves for different silver loadings in linear (a) and semi-logarithmic (b) representation.

electrochemical reaction, thus the length of the reaction zone corresponds to the effective electrolyte intrusion depth. In principle the length of the diffusion layer could influence the oxygen transport and thus the oxygen availability at the reaction zone. However, longer diffusion lengths in the gas phase barely influence the overall polarization characteristics, as the transport in the gas phase is much faster than in the liquid phase. Therefore, we assume that the electrodes performance is primarily defined by the effective intrusion depth and that other effects are negligible. The full nickel electrode is neglected in this analysis. The resulting polarization curves are shown in Figure 4. For the full silver electrode (136 $mg_{Ag}\,cm^{-2}$) two cases, intrusion of the electrolyte over the full and over half the electrode thickness, are considered. A fair agreement between experiment and simulation is reached concerning the linear region and limiting current density, the assumption of a full intrusion represents the experiments slightly better at this point. In the kinetic region, a rather large deviation is evident assuming a full intrusion. The gap between experiment and simulation reduces with decreased intrusion depth of the electrolyte. However, it has to be noted that the model was not parameterized to the exact half-cell conditions and electrolyte concentration used in the experiment. We can therefore conclude that the intrusion depth of the electrolyte in a full silver electrode is most likely between half and full thickness of the GDE, as already proposed in our previous publication.[7] For the higher loadings above 35 $mg_{Ag}\,cm^{-2}$ the trend of the simulation matches the experiment quite well. However, the predicted limiting current densities are slightly higher than during the experiments. For the loadings of 15 and 30 $mg_{Ag}\,cm^{-2}$, the simulation does not fit the experimental data with the predicted limiting current density being up to three times higher than in the experiment. This indicates either that there is another resistance in the GDE system, which is not yet included in the model, or that the available reaction zone is smaller than assumed. In the kinetic region a qualitative agreement between model and experiment is reached. The exact values are not met, but the presumed trend of lower overpotentials with increased silver loading is correctly represented, especially for loadings of 15, 30 and 45 $mg_{Ag}\,cm^{-2}$, respectively. Additionally, the applied Tafel kinetics are invalid at overpotentials above approx. −50 mV indicated by the grey shaded area in the semi-logarithmic representation. Deviations between simulation and experiments in this range are to be expected.

In the second attempt, the length of the reaction layer, i.e. the effective intrusion depth of the electrolyte, is used as a fitting parameter for each electrode and determined via a least squares fit. All other parameters and process variables are kept constant. In this case the full silver electrode is neglected. In Figure 5 the determined reaction lengths and resulting polarization curves compared to the experimental data are shown. Except for a silver loading of 30 $mg_{Ag}\,cm^{-2}$ the model-based analysis is in good agreement with the calculations utilizing the density and the thickness gauge measurements. For loadings above 35 $mg_{Ag}\,cm^{-2}$ the maximum deviation to the results of one of these methods is only 5 µm, whereas it rises up to 10 µm for a loading of 15 $mg_{Ag}\,cm^{-2}$. As the only outlier remains a loading of 30 $mg_{Ag}\,cm^{-2}$ where the difference almost reaches 20 µm. The resulting polarization curves now show a fair agreement with the experimental data. In all cases, the limiting current densities are predicted correctly and for catalyst loadings of 35 and 40 $mg_{Ag}\,cm^{-2}$, even a quantitative match is obtained.

These experiments combined with the model-based analysis allow a prediction of the active area of GDE. However, there are still some uncertainties regarding the employed parameters in the model. As the half-cell experiments are carried out in the commercially available half-cell, the stagnant electrolyte film in front of the electrode may be thicker than in the flow cell

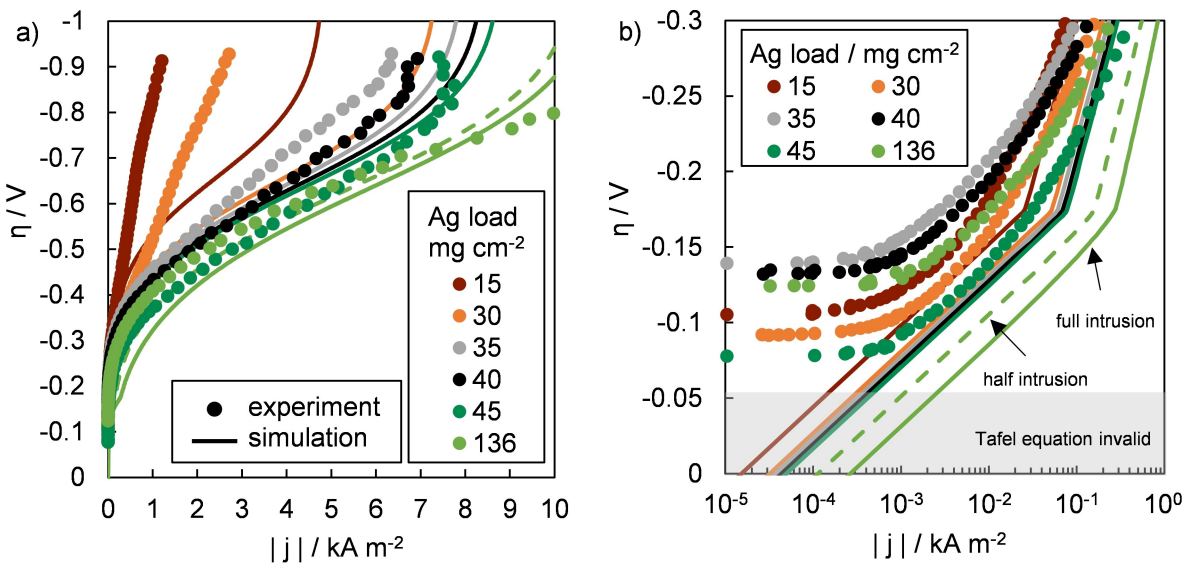


**Figure 4.** Experimentally determined and simulated polarization curves for graded and full silver electrodes in linear (a) and semi-logarithmic (b) representation.

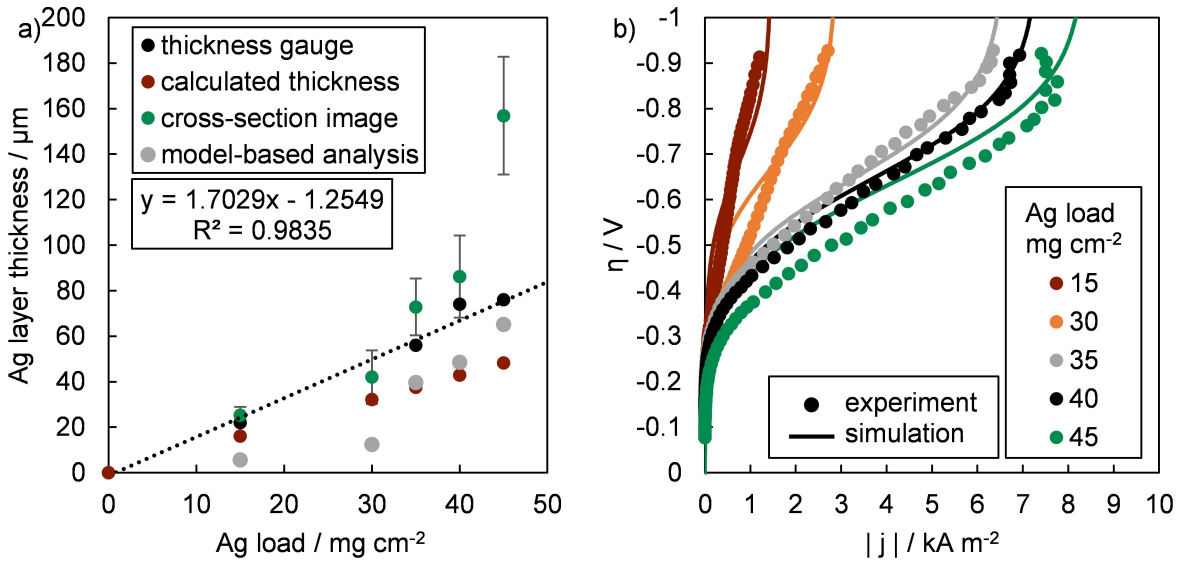


**Figure 5.** Silver layer thickness determined by experiments and model-based analysis (a), and resulting polarization curves (b) as a function of the silver loading.

utilized in our previous publication.[7] This influences the diffusion lengths of the liquid species and thus the limiting current density in the model. Further, we assumed that the gas transport in the nickel structure is not inhibited by a possible presence of electrolyte in the pore system. However, considering such effects would increase the number of model parameters as well as the uncertainties and thus would require a new parameterization process of the system. Overall, the experiments and the model-based analysis reveal the key importance of the electrolyte distribution inside the electrodes and how the overall performance is influenced.

## 3. Conclusions

In this study, we developed graded electrodes to determine the catalytically active area of GDEs during ORR experimentally. In contrast to former approaches using barrier layers,[18] the division into nickel and silver layers allows an exact prediction of the active part of the electrodes. In an optimized manufacturing process, nickel transport layers were coated with silver catalyst of uniform thickness. We determined the silver layer thickness by a thickness gauge, weighing and verified it by analyzing cross-section images. These thicknesses were implemented in our TFFA-model as the length of the reaction layer. In this model-based analysis, we obtained similar effective penetration depths of the electrolyte. However, due to the manufacturing process we are limited to a maximum catalyst layer thickness of 75 µm in order to ensure the equivalence of the individual electrodes. Experimental data for higher reaction lengths in graded electrodes is not available. Even if a fabrication of catalyst layers thicker than 75 µm was possible, the resulting polarization curves would merge, making it difficult to differentiate between single electrodes. Comparing the graded electrode with the highest silver loading (45 $mg_{Ag}\,cm^{-2}$) and the full silver electrode, there is still a significant difference in the limiting current density. This proves, that the active part of the full silver electrode is thicker than 75 µm and thus the electrolyte must intrude much deeper than expected from other simulation approaches.[15–17] Unfortunately, the electrolyte penetration depth cannot be determined exactly for the full silver electrode and will only be revealed by operando tomography experiments. Nevertheless, we proved experimentally and with our model-based analysis that large parts of the full silver GDE are intruded by the electrolyte and are utilized for the ORR in high alkaline media.

## Experimental Section

### Electrode preparation

The electrodes are prepared batch wise by means of a wet spraying process inspired by the work of Moussallem et al.[13] and described in detail in previous publications.[20,21] A metal containing suspension is sprayed on a nickel mesh (106 µm × 118 µm mesh size, 63 µm wire thickness, Haver & Boecker OHG) as support and conducting agent using an airbrush gun (Evolution, 0.6 mm pin hole, Harder & Steenbeck). A heating table allows to simultaneously dry each layer while being applied resulting in a homogeneous electrode surface. The spraying process is completed when a total metal loading of approx. 130 $mg_{Me}\,cm^{-2}$ is reached. Mechanical stability is increased by subsequent hot pressing (LaboPress P200S, Vogt, 15 MPa, 130 °C) and sintering in an air furnace (15 min, 330 °C), during which the final pore system is formed.

For the nickel layer a suspension consisting of 30 g nickel powder (Ni 99.9%, APS 3–7 µm, Alfa Aesar), 30 g hydroxyethyl methyl cellulose (1 wt% solution, WALOCEL™ MKX 70000 PP01) as thickener and pore building agent, a PTFE dispersion (TF 5060GZ, 3 M™ Dyneon™) and 40 g demineralized water is mixed. The sprayed electrodes are hot pressed (58 MPa, 130 °C) in an intermediate step to ensure a smooth surface for the silver coating. This ensures a uniform thickness of the silver layers. For the

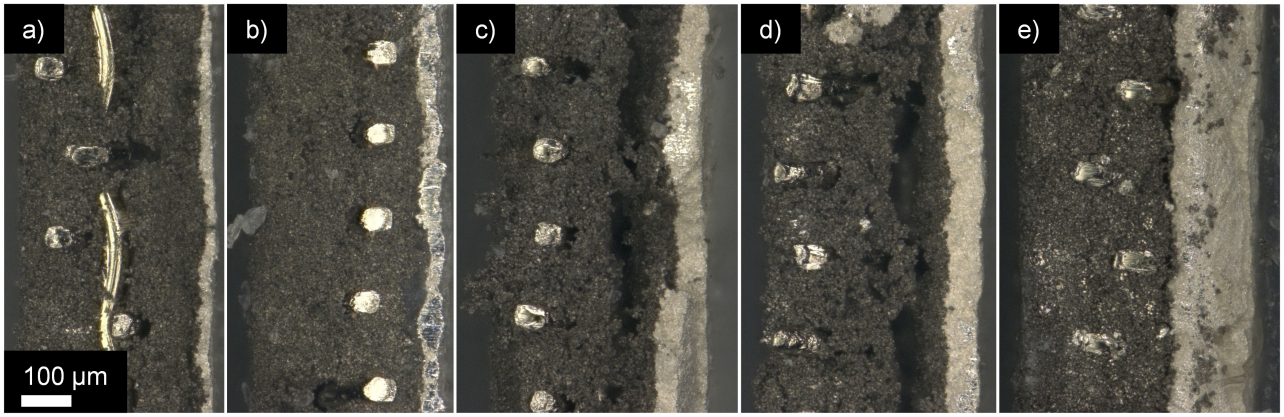


**Figure 6.** Cross-section images of graded nickel/silver electrodes with 15 (a), 30 (b), 35 (c), 40 (d) and 45 $mg_{Ag}\,cm^{-2}$ (e) loading. The bright layers are silver, the dark areas nickel. In the center, the nickel mesh support is visible.

catalytically active layer a suspension consisting of 30 g silver flakes (SF9ED, Ames Advanced Materials Corp.), 50 g hydroxyethyl methyl cellulose, PTFE dispersion and 40 g demineralized water is mixed. The suspension is applied on one side of the previously prepared nickel electrodes until the desired silver loading is obtained. Afterwards the described processing steps are performed and the final electrode is reached. All electrodes layers, nickel and silver, consist of 97 wt% metal and 3 wt% PTFE. For comparison, a pure nickel and a pure silver electrode are also produced.

### Physical characterization

The median thickness of the silver layers are determined from nine measurements using a thickness dial gauge (FD 50, Käfer GmbH) before the coating and after final sintering. Additionally, the layer thickness is calculated using the silver loading and the true density of pure silver GDE determined in a former study.[20] Loadings are determined by weighing, taking the average weight loss during the sintering process into account. After electrochemical experiments, layer thicknesses are verified through cross-section images (see Figure 6) using a 3D microscope (VHS-2000D, Keyence). Before cutting, the electrodes were frozen using liquid nitrogen to prevent the silver layers from deformation. Flow-through pores are determined using capillary-flow porometry (Porometer 3G, Quantachrome). On top of the probe a wetting fluid (Porofil, Quantachrome) is applied. Inside the device, the fluid is driven out of the pores using a pressure gradient while the nitrogen flow rate is detected. A comparison of nitrogen flow through the wet and dry probe provides the pore size distribution.

### Electrochemical characterization

Electrochemical experiments are performed in a commercially available half-cell (FlexCell HZ-PP01, Gaskatel GmbH) at 80 °C utilizing an effective surface area of 3.14 $cm^2$. As electrolyte 30 wt% NaOH solution prepared from caustic flakes ($\geq$ 99 wt%, Carl Roth) and demineralized water is used. Dry oxygen is supplied with a flow rate of 50 $mL\,min^{-1}$ and backpressure using a 1 mm water column at the outlet. Potentials are measured using a three-electrode configuration, with the GDE as working, a platinum wire as counter and a reversible hydrogen electrode (RHE), connected through a Luggin-capillary, as reference electrode with a Reference 3000™ potentiostat (Gamry Instruments). The standard potential of the oxygen reduction reaction (ORR) vs. RHE at the given conditions is 1.13 V, calculated by the method introduced in a previous publication.[20] The dependence of the potential on temperature,[22] activity of water[23] as well as hydroxide ions[24] and the actual oxygen concentration in the electrolyte[3] is considered in the corresponding Nernst equation.

In a start-up procedure, constant current densities (1, 2, 3 and 4 $kA\,m^{-2}$) are applied for 5 minutes each, followed by pseudo-galvanostatic impedance spectroscopy (1 $kA\,m^{-2}$, 5 mV amplitude) (not shown). The electrode performance is finally investigated by *iR*-compensated (current interrupt method) linear sweep voltammetry (LSV) measurements starting at open cell potential (OCP) to 200 mV vs. RHE with a scan rate of 0.5 $mV\,s^{-1}$.

### TFFA model description

The TFFA model used to analyze the experiments is described in detail in our previous publication.[7] Maxwell-Stefan diffusion equations are used to describe the gas and liquid transport. The required diffusion coefficients are calculated according to Fuller et al.[25] for the gas phase and as described in Newman et al.[26] for the liquid phase. It is assumed that the liquid electrolyte penetrates the GDE forming a finger-shaped distribution creating the reaction layer. Gas and liquid transport take place simultaneously in the reaction layer. Electrolyte properties, such as vapor pressure,[23] Henry constant,[3] activity of NaOH[24] and water[23] are spatially resolved. Oxygen can dissolve anywhere on the electrolyte finger. The reaction is described according to Tafel kinetics[27] coupled with a classical reaction engineering approach allowing to calculate the concentration profile of oxygen inside the electrolyte finger.[28]

No changes regarding the parameter set are made, and only the boundary conditions are adapted to the experimental setup. In the first attempt, the determined silver layer thickness of each electrode is implemented as the reaction layer length and total intrusion depth of the electrolyte. In the second attempt, the length of the reaction layer is treated as a fitting parameter to achieve the best possible description of the measured results. A schematic overview of the model is shown in Figure 7. The complete model code, including all equations and parameters, is provided in the supporting information.

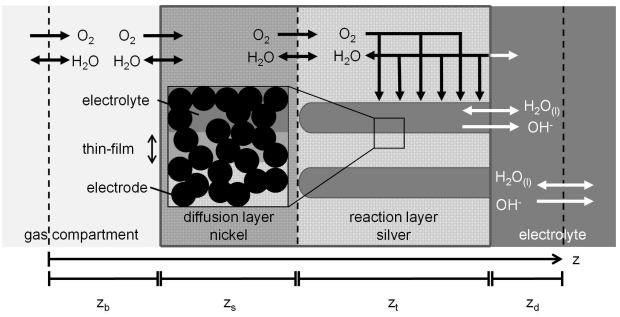


**Figure 7.** Scheme of the used TFFA model.

## Acknowledgements

*The authors acknowledge financial support for this study by Deutsche Forschungsgemeinschaft in the framework of the research unit "Multiscale analysis of complex three-phase systems: Oxygen reduction at gas-diffusion electrodes in aqueous electrolyte" (FOR 2397; research Grant TU 89/13-1). Open access funding enabled and organized by Projekt DEAL.*

## Conflict of Interest

The authors declare no conflict of interest.

**Keywords:** gas-diffusion electrode · oxygen reduction reaction · graded electrode · modelling · electrolyte distribution

[1] J. Kintrup, M. Millaruelo, V. Trieu, A. Bulan, E. S. Mojica, *Electrochem. Soc. Interface* **2017**, *26*, 73.
[2] "Chlor-Alkali Electrolyis", https://ucpcdn.thyssenkrupp.com/_legacy/UCPthyssenkruppBAISUhdeChlorineEngineers/assets.files/products/chlor_alkali_electrolysis/thyssenkrupp_chlor_alkali_brochure_web.pdf.
[3] D. Tromans, *Hydrometallurgy* **1998**, *50*, 279.
[4] N. Furuya, H. Aikawa, *Electrochim. Acta* **2000**, *45*, 4251.
[5] M. Gebhard, M. Paulisch, A. Hilger, D. Franzen, B. Ellendorff, T. Turek, I. Manke, C. Roth, *Materials* **2019**, *12*.
[6] M. C. Paulisch, M. Gebhard, D. Franzen, A. Hilger, M. Osenberg, N. Kardjilov, B. Ellendorff, T. Turek, C. Roth, I. Manke, *Materials* **2019**, *12*.
[7] D. Franzen, M. C. Paulisch, B. Ellendorff, I. Manke, T. Turek, *Electrochim. Acta* **2021**, 137976.
[8] M. B. Cutlip, *Electrochim. Acta* **1975**, *20*, 767.
[9] X.-L. Wang, S. Koda, *Denki Kagaku* **1997**, *65*, 1002.
[10] X.-L. Wang, S. Koda, *Denki Kagaku* **1997**, *65*, 1014.
[11] S. Pinnow, N. Chavan, T. Turek, *J. Appl. Electrochem.* **2011**, *41*, 1053.
[12] P. Jeanty, C. Scherer, E. Magori, K. Wiesner-Fleischer, O. Hinrichsen, M. Fleischer, *J. $CO_2$ Util.* **2018**, *24*, 454.
[13] I. Moussallem, S. Pinnow, N. Wagner, T. Turek, *Chem. Eng. Process.* **2012**, *52*, 125.
[14] P. Frania, *Herstellung, Analyse und Optimierung von Sauerstoffverzehrkathoden mit elektrochemisch abgeschiedenem Silberkatalysator zum Einsatz in der Chlor-Alkali-Elektrolyse*. Dissertation, 1st ed., Verlag Dr. Hut, **2016**.
[15] P. Kunz, M. Paulisch, M. Osenberg, B. Bischof, I. Manke, U. Nieken, *Transp. Porous Media* **2020**, *132*, 381.
[16] M. Röhe, F. Kubannek, U. Krewer, *ChemSusChem* **2019**, *12*, 2373.
[17] M. Röhe, A. Botz, D. Franzen, F. Kubannek, B. Ellendorff, D. Öhl, W. Schuhmann, T. Turek, U. Krewer, *ChemElectroChem* **2019**, *6*, 5671.
[18] M. Gebhard, T. Tichter, D. Franzen, M. C. Paulisch, K. Schutjajew, T. Turek, I. Manke, C. Roth, *ChemElectroChem* **2020**, *7*, 830.
[19] S. N. S. Goubert-Renaudin, A. Wieckowski, *J. Electroanal. Chem.* **2011**, *652*, 44.
[20] D. Franzen, B. Ellendorff, M. C. Paulisch, A. Hilger, M. Osenberg, I. Manke, T. Turek, *J. Appl. Electrochem.* **2019**, *49*, 705.
[21] M. Koj, J. Qian, T. Turek, *Int. J. Hydrogen Energy* **2019**, *44*, 29862.
[22] S. G. Bratsch, *J. Phys. Chem. Ref. Data* **1989**, *18*, 1.
[23] J. Balej, *Int. J. Hydrogen Energy* **1985**, *10*, 233.
[24] J. Balej, *Collect. Czech. Chem. Commun.* **1996**, *61*, 1549.
[25] E. N. Fuller, K. Ensley, J. C. Giddings, *J. Phys. Chem.* **1969**, *73*, 3679.
[26] J. Newman, D. Bennion, C. W. Tobias, *Berich. Bunsen. Gesell.* **1965**, *69*, 608.
[27] S. Kandaswamy, A. Sorrentino, S. Borate, L. A. Živković, M. Petkovska, T. Vidaković-Koch, *Electrochim. Acta* **2019**, *320*, 134517.
[28] P. Björnbom, *Electrochim. Acta* **1987**, *32*, 115.

Manuscript received: March 3, 2021
Revised manuscript received: March 30, 2021
Accepted manuscript online: April 1, 2021